AIAA Propulsion and Energy Forum
19-22 August 2019, Indianapolis, IN
AIAA Propulsion and Energy 2019 Forum

10.2514/6.2019-3901

Data-driven Scaling Law for the Extractor Current of a Capillary Electrospray

Peter N. Dahl,[1] Angela M. Kimber[1], and Benjamin A. Jorns[2]
University of Michigan, Ann Arbor, MI, 48109, USA

An experimental investigation into the impingement current on the extractor electrode of a capillary electrospray is presented. This is a critical parameter that impacts both thrust production and lifetime of this device. A semi-empirical scaling law for the dependence of this extractor current on extractor voltage and total beam current is derived from first principles. This model is then evaluated by comparing its predictions to the measured extractor current from a single pressure-fed capillary operating on EMI-BF4. The comparison is performed over a parametric range of discharge voltage (1400-2000 V), mass flow rate (0.25 to 0.67 nl/s), and distance from capillary to extractor (0.7-1.5 mm). For a fixed extractor-to-capillary distance, this scaling law is shown to exhibit both quantitative and qualitative agreement within a scaling factor with measurements. This scaling factor in turn is observed to change as the extractor distance is varied. An empirically-based analytical equation for this dependence on extractor distance is proposed and used to modify the scaling law. The resulting expression for extractor current is validated against experiment data and is discussed in the context of how it may be used to evaluate electrospray lifetime and performance.

I. Nomenclature

c_1	=	scaling coefficient
d	=	emitter-to-extractor distance
E_r	=	radial electric field within plume
I_B	=	beam current
I_E	=	current incident on extractor
K	=	fluid electrical conductivity
m	=	droplet mass
$\dot{m}$	=	rate of propellant accumulation on extractor electrode
N	=	particles present in discrete slice of plume
Q	=	volumetric propellant flow rate
q	=	droplet charge
r	=	radial position
r_e	=	capillary radius
V_C	=	applied extraction voltage
V_S	=	minimum onset voltage
v_z	=	droplet axial velocity
w	=	extractor aperture width
z	=	axial position
γ	=	fluid surface tension coefficient
ϵ	=	fluid dielectric constant
ε_0	=	permittivity of free space

[1] Graduate student, Department of Aerospace Engineering
[2] Assistant Professor, Department of Aerospace Engineering; AIAA Senior Member

θ = plume divergence angle
ϕ = emitter/extractor line-of-sight angle

II. Introduction

Electrospray thrusters, also called colloid thrusters, are electric propulsion (EP) devices that use an electric field to accelerate an ionic fluid and generate thrust. They are a particularly promising form of electric propulsion because of their high theoretical limits for efficiency and thrust density. Unlike most EP systems, electrospray thrusters do not require the ionization of a neutral gas before accelerating their propellant. Thrust can be generated simply by applying a sufficiently strong electric field to extract charge carriers directly from the conducting fluid propellant [1,2]. Since electrospray thrusters typically lose only 0.5% of total energy to this extraction process (as compared to 10-30% ionization losses on alternative forms of EP devices), these systems are expected to exhibit higher efficiency [3] while still maintaining comparable specific impulse to other EP concepts [4]. The major drawback of these devices is their low thrust — individual electrospray thruster emitters only produce tens to hundreds of nanonewtons [5-7]. While this thrust level is sufficient for micro-scale stationkeeping applications [8], it is too low for most maneuvering requirements in space. Indeed, electrospray thrusters can only produce comparable levels of thrust to other forms of EP if they are multiplexed — an architecture where hundreds or thousands of closely-packed emitters are arrayed and fired simultaneously.

Before these types of array architectures can be realized, there are a number of practical challenges and questions about the operation of electrospray thrusters that must be resolved [8]. One of the most critical of these is the risk posed to thruster lifetime by propellant accumulation on the downstream extractor and accelerating electrodes. This process is a well-known and dominant life-limiting factor for electrospray thrusters [9] as the propellants used typically have no measurable vapor pressure [10]. Fluid thus cannot evaporate from the electrodes once it has been deposited. If a sufficient amount of fluid accumulates on these electrodes, arcing events in the grid gaps can onset which ultimately disable the device [11]. This was believed to be a failure mode experienced by one of the electrospray thrusters on the recent Space Technology 7 (ST-7) Disturbance Reduction System that supplied precision attitude control for the LISA Pathfinder mission [12].

While it is possible to mitigate the problem of propellant accumulation with carefully-manufactured individual emitters, this solution is not practical or translatable to the arrays of potentially thousands of emitters necessary to generate higher levels of thrust. Challenges in manufacturing tolerance and alignment prohibit the necessary tailoring of individual emission sites to inhibit propellant accumulation. Instead, it has become common practice to build prototype arrays to the highest precision possible and evaluate lifetime through direct testing. This method, although unambiguous, can be both time- and cost-prohibitive. As a faster, more cost-effective alternative, numerical modeling is becoming an increasingly important tool to assess the viability of electrospray concepts [4,9,13-15]. Recent numerical efforts in particular have focused on developing engineering toolkits [16] that leverage semi-empirical, analytical scaling laws for electrospray operation. This approach has the advantage of being able to facilitate rapid statistical evaluation of electrospray configurations with known tolerances and alignment uncertainties.

While these types of simple engineering-based frameworks have already demonstrated the ability to predict key parameters such as electrospray performance, to date, they have only had a limited capability to evaluate lifetime. This stems from the fact that scaling laws are not readily available for the propellant accumulation on the downstream electrodes. In light of this limitation, the goal of this work is to develop an experimentally-validated model for a parameter that can serve an approximate proxy for this mass accumulation: the current collected by the extractor electrode. As such, this paper is organized in the following way. We first establish a scaling law from first principles for this collected current. We then describe our experimental setup and diagnostic system to generate data to both calibrate and validate this scaling law. Finally, we present the experimental results of the calibration, validate the predictions of the resulting scaling law against measurements, and discuss the limitations and implications of our results for electrospray modeling.

III. Model for extractor impingement

We derive in this section from first principles an analytical expression for the current impingement on the extractor electrode for a pressure-fed capillary-based electrospray emitter. We show in Fig. 1 a canonical geometry that we reference for this derivation. In this axisymmetric configuration, an applied upstream pressure induces flow of ionic liquid through a hollow capillary emitter with radius r_e. In the absence of applied electric field, this ionic

liquid pools into a hemispherical meniscus at the capillary end. During operation, a strong potential, V_C, applied between a concentrically aligned downstream extractor electrode at a distance d and the conducting ionic fluid deforms the meniscus into a Taylor cone shape. From the micrometer tip of this Taylor cone, droplets — and in some cases, ions — can be extracted by the applied field [2].

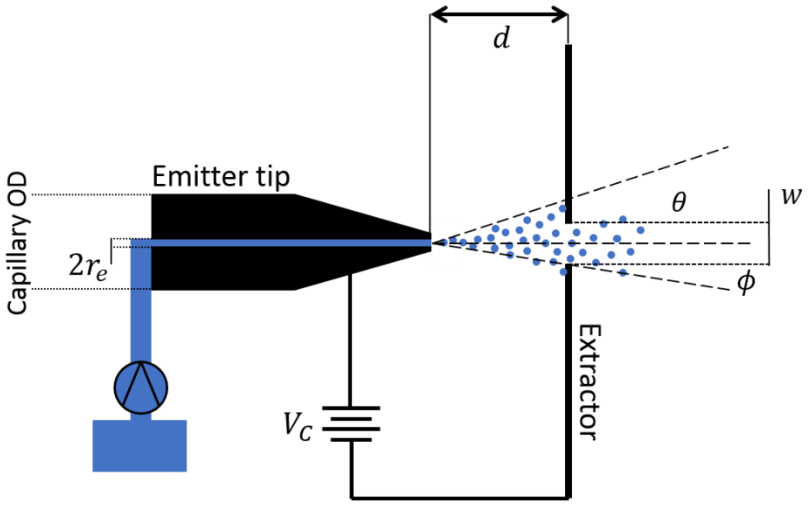

Figure 1: Emitter geometry showing emitter inner diameter $2r_e$, extractor gap d, applied voltage V_C, extractor diameter, and solid angle subtended by the extractor aperture. As divergence angle θ exceeds the line-of-sight angle ϕ to the extractor aperture, propellant impinges on the grid.

The emitted spray from capillary electrosprays can occur in several modes depending on the applied potential and fluid flow rate [11]. Cone-jet mode is characterized by a single Taylor cone with a continuous jet originating from its tip; this jet then breaks up into charged droplets farther downstream, yielding a plume of propellant. Other emission modes may include dripping, multi-jet emission mode [11], and pure ionic emission [14]. For the test article configuration we examine in this study, where there is a high flow of propellant, the spray operates primarily in the single cone-jet mode with droplet emission. We therefore confine our discussion to this class of plume.

As is shown qualitatively in Fig. 1, the emitted droplet stream from the capillary spreads as the propellant is drawn toward the extractor. If this spread is larger than the width of the extractor orifice, a fraction of the beam will impact the electrode. This in turn gives rise to mass accumulation, $\dot{m}$, on this surface that can lead to failure modes for these devices. While it is difficult to determine the magnitude of mass accumulation rate in situ, we can relate it approximately to the more easily measured current, I_E, that is collected by this electrode with the relation $\dot{m} \approx (m/q)\, I_E$, where q and m denote the droplet charge and mass respectively. This scaling relationship is contingent on the assumption that the beam generated by the electrospray is mono-dispersive with a fixed mass-to-charge ratio. While in reality this scaling is not exact as the actual electrospray beam is probably poly-dispersive, this relationship shows that the collected extractor current is a qualitatively valid proxy for the actual mass deposition.

With this in mind, we can derive from first principles an approximation for this beam current if we make the following simplifying approximations:

- The total current generated by the electrospray, I_B, expands into a cone of constant solid angle characterized by divergence angle, θ, (Fig. 1)
- The current density along the surface of the expanding cone at a fixed radial distance from the tip is normal to the cone surface and constant.

Subject to these assumptions, we can find an expression for the ratio of the current collected on the extractor to the total beam current as

$$\frac{I_E}{I_B} = \frac{cos\,\phi - cos\,\theta}{1 - cos\,\theta}, \tag{1}$$

where we have defined the angle subtended by the exit extractor as $\tan\phi = \frac{w}{2d}$. Here w denotes the diameter of the extractor aperture. Physically, this relationship shows that if the characteristic divergence of the plume is smaller than the angle subtended by the extractor hole ($\theta < \phi$), there will be no extractor impingement ($I_E/I_B \rightarrow 0$). Conversely, as the divergence angle increases, an increasingly larger fraction of the emitted current from the tip will be intercepted on the grid.

While Eq. (1) expresses the extractor current as a function of the extractor geometry, in order to arrive at a closed form solution, it is necessary to find a result for the divergence angle, θ, that depends on the operating conditions of the emitter. To this end, we consider here the simplified expression for extractor divergence proposed by Lozano [14]. In this formulation, the dominant mechanism governing the beam divergence is assumed to be the radial electric field that results from space charge effects between the droplets in the beam [13,14]. For a mono-dispersive droplet beam (as is consistent with our assumptions outlined above), this space charge effect yields the result

$$\theta \approx tan^{-1}\left(\frac{9}{2}\left(\frac{I_B}{2\pi\varepsilon_0}\sqrt{\frac{m}{2q}}V_C^{-\frac{3}{2}}\right)^{\frac{1}{2}}\right), \tag{2}$$

where ε_0 is the permittivity of free space. This expression depends on measurable parameters — beam current and extractor voltage — as well as the less easily-defined charge to mass ratio. We can eliminate this latter value if we again assume (as is consistent with our above approximations) that the beam is mono-dispersive. This allows us to write $m/q \propto Q/I_B$, where Q denotes the flow rate. Finally, we can leverage the empirical result from de la Mora [17] who showed that for typical pressure-fed capillary systems operating in droplet mode, the beam current can be related to the flow rate via

$$I_B = f(\epsilon)\sqrt{\frac{\gamma Q K}{\epsilon}}, \tag{3}$$

where ϵ and K are the dielectric constant and the electrical conductivity of the liquid, γ is the coefficient of surface tension, and $f(\epsilon)$ is an empirical function. Armed with Eq. (3) and the assumption that the flow is mono-dispersive, we thus find the simplified result

$$\theta \approx \tan^{-1}\left(\left(R_0(P)\frac{I_B}{V_C}\right)^{\frac{3}{4}}\right), \tag{4}$$

where we have condensed all the constants and the dependence on the properties of the propellant (e.g., ϵ, K, etc.) into a characteristic resistance

$$R_0(P) \approx \left(\frac{9}{2}\right)^{4/3}\left(\frac{1}{2\sqrt{2}\,\pi\varepsilon_0 f(\epsilon)}\sqrt{\frac{\epsilon}{\gamma K}}\right)^{2/3} \tag{5}$$

that has units of Ohms. Physically, we see from Eq. (4) the intuitive dependence of the divergence on operating conditions. As the beam current increases, there are more charge carriers, which results in a larger space charge field forcing the beam to diverge. Similarly, as the extractor voltage increases, the force in the axial direction is larger, collimating the beam.

Although the simplified form of Eq. (4) for divergence angle is compact and self-consistent, its derivation neglects a number of key features which may also have a weak influence on divergence. The most notable example is the tip-to-extractor distance, d. Physically, we may expect there to be some dependence on this spacing due to its influence on the axial electric field experienced by the droplets between emitter and extractor. It does not appear in Eq. (4), however, because the derivation of this result assumes that there is negligible electric field downstream of the Taylor cone tip. In an effort to account for the possibility of this parameter influencing the divergence angle, we adopt the approach of folding this dependence into a leading coefficient $c_1(d)$ with an explicit but unknown dependence on extractor distance:

$$\theta \approx \tan^{-1}\left(c_1(d)\left(R_0(P)\frac{I_B}{V_C}\right)^{\frac{3}{4}}\right). \tag{6}$$

By combining this result with Eq. (1), we thus have an analytical expression for the estimated extractor current with only one free parameter. The goal in the next section is to generate an experimental database for an actual capillary emitter to evaluate this expression and calibrate its fit coefficient c_1.

IV. Experimental Setup

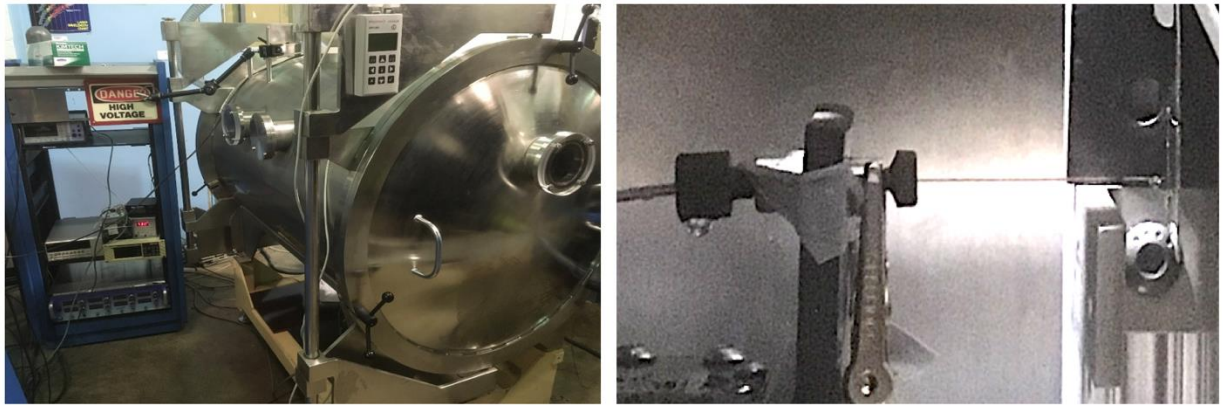

Figure 2: Electrospray Thruster Array Chamber (left) and the pressure fed capillary and extractor experimental setup (right).

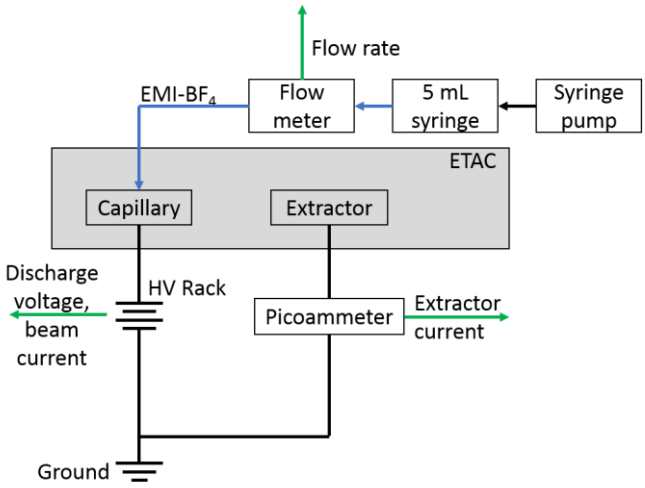

Figure 3: Schematic of experimental setup indicating power supplies, flow system, and diagnostics.

We conducted experiments to generate the required datasets for model calibration at the University of Michigan's Plasmadynamics and Electric Propulsion Laboratory (PEPL). Fig. 2 shows an external view of the Electrospray Thruster Array Chamber (ETAC), a 1-meter-diameter by 1.2-meter-long long steel test chamber, and a close-up view of the experimental setup consisting of a single-emitter pressure-fed capillary. The electrospray device consisted of a fused-silica emitter tip which tapered to a tip diameter of 8 μm and a translating aluminum extractor plate with a 2 mm-diameter hole. This latter electrode was aligned to be concentric with the capillary tube and was mounted on a micro translation stage capable of varying distance from the capillary between 0.7 mm and 1.5 mm. 1-ethyl-3-methylimidazolium tetrafluoroborate (EMI-BF4) was used as propellant and was delivered to the emitter by a flow system consisting of a mechanical syringe pump, a 5 mL syringe, and lengths of PEEK tubing with inner diameters of 0.15 mm and 0.25 mm. Current emission from the liquid meniscus that formed at the end of the capillary was induced by applying an electrical potential between the extractor plate and the ionic liquid. The electrical connection to the propellant was made via an electrode placed immediately upstream of the capillary and in series with the PEEK tubing. Throughout the experimental campaign, the chamber was held at 10^{-4} Torr vacuum by a turbomolecular pump.

During testing, the flow rate, voltage from extractor to capillary, and distance were varied as we measured both the total current and the current collected on the extractor. Figure 3 shows a schematic for the diagnostics, telemetry, and control systems. The extraction voltage was supplied by an UltraVolt "HV Rack" high-voltage power supply, which also measured beam current I_B via an internal, calibrated current sensor. The propellant flow rate was determined via an ECO-Nano-1X CorSolutions flow meter calibrated for EMI-BF4. Current incident on the extractor plate was measured by a Keithley 6485 pico-ammeter.

V. Results

In order to evaluate the model proposed in Section III, we measured the extractor current and beam current over a wide range of operating conditions (Table 1). With the values from this parametric investigation, we then were able to use the formulations from Eqs. (1) and (6) to calculate the calibration coefficient, $c_1(d)$. The resulting dependence is shown in Fig. 4, where we have distinguished the datasets based on flow rate. Here we have used typical values for EMI-BF4 extracted from the online resource, the Electrospray Propulsion Engineering Toolkit [19] (Table 2) to estimate a propellant characteristic resistance of R_0 =47.7 kΩ (for simplicity, we have assumed the empirical coefficient $f(\epsilon) = 1$). We also note that we only report values where we could achieve a stable spray and measure extractor currents in excess of 5 nA. This was the minimum threshold that we could resolve above the noise of our diagnostic. While there were conditions where the extractor current was in this noise floor, it is assumed that in these cases the divergence angle was close to or narrower than the angle subtended by the extractor — leading to a low intercepted current. We similarly note that there are fewer data points for the higher flow cases with a shorter range of extractor voltage. This is because the range of stable operation was curtailed at these higher flows.

Table 1: Investigated range of input conditions for the electrospray emitter.

Quantity	Minimum	Maximum	Step
V_C	1400 V	2000 V	25 V
d	0.7 mm	1.4 mm	0.1 mm
Q	0.25 nL/s	0.67 nL/s	Variable

There are two notable features from the results shown in Fig. 4. The first is that there is an evident inverse relationship between the calibration coefficient and extractor distance. This suggests that we were correct in Sec. III in hypothesizing that the geometry should also have a role in driving the beam divergence. Indeed, in the context of Eq. (6), we see the divergence angle decreases as the extractor distance is widened. This, physically, is intuitive as increasing distance gives rise to more collimated electric field between the emitter and extractor, thus in principle producing a more collimated beam. The second feature that we note is that although multiple conditions were experimentally characterized, there appears to be a well-defined trend in the data — one that may potentially be fit by an empirical function.

Table 2: EMI-BF4 properties for evaluating R_0 at a temperature of 298 K.

Quantity	Value
K	1.390 S/m
γ	0.050 N/m
ϵ	12.9 ϵ_0

For the purpose of making the analytical model we proposed in Sec. III predictive, we consider two candidate functions to fit this data. These expressions and their best-fit coefficients (determined from a sum of residuals analysis) are shown in Table 3 and plotted against the data in Fig. 4. The first function we consider is linear, as this is one of the simplest analytical forms that qualitatively matches the data. The second function we consider is

informed by physical intuition: namely, we choose a form that scales in the same way as the other dependencies in Eq. (6) — that is, to the 3/4 power. Comparing these functions to the data in Fig. 4, we see that they exhibit both qualitative and quantitative agreement with the data over the parameter space of investigated conditions.

We in turn can evaluate the ability of these functional forms to allow the combination of Eqs. (1) and (6) to predict the extractor current. To this end, we show in Fig. 5 response plots for the measured ratio of extractor current to beam current compared to the predicted value that we determined from the formulations in Sec. III and the two empirical functions shown in Table 3. For reference, a perfect model in these response plots would yield all data points falling on the shown dotted line (i.e., with a 1-to-1 correspondence). As can be seen from these figures, the empirical functions combined with the model from Sec. III yield predictions that approximately follow the ideal response. While they both exhibit deviations at low ratios including negative currents (an artifact discussed in the following section), they show improved predictive capability as the fraction of extractor current increases. We similarly see that the second empirical function, with the inverse dependence on the extractor distance, yields the qualitatively greater agreement with the measured data.

Table 1: Proposed functional forms for $c_1(d)$ with best fit coefficients.

Function	a	b
$a * d + b$	-5.0×10^{-4}	1.0×10^{-3}
$(a/d)^{3/4}$	4.2×10^{-5}	-

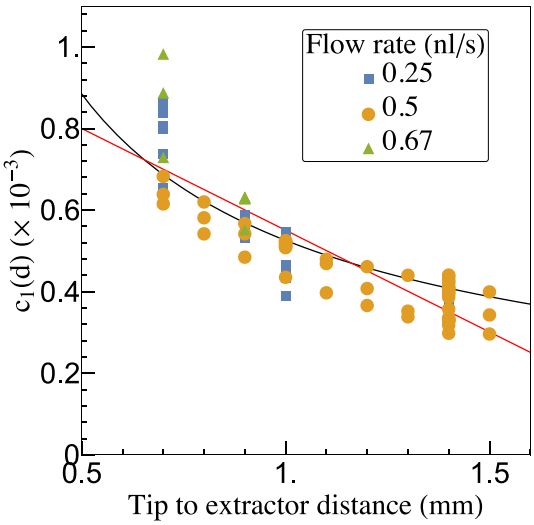

Figure 4: Calibration coefficient from Eq. 5 inferred from experimental data for three different flow rates. Extractor voltage and beam current varied from 1450 V to 2000 V and 700 nA to 2300 nA for the 0.25 nl/s case; 1450 V to 1910 V and 816 nA to 2660 nA for the 0.5 nl/s case; and 1500 V to 1850 V and 710 to 1120 nA for the 0.67 nl/s case. Two empirical fit functions from Table 3 are also shown.

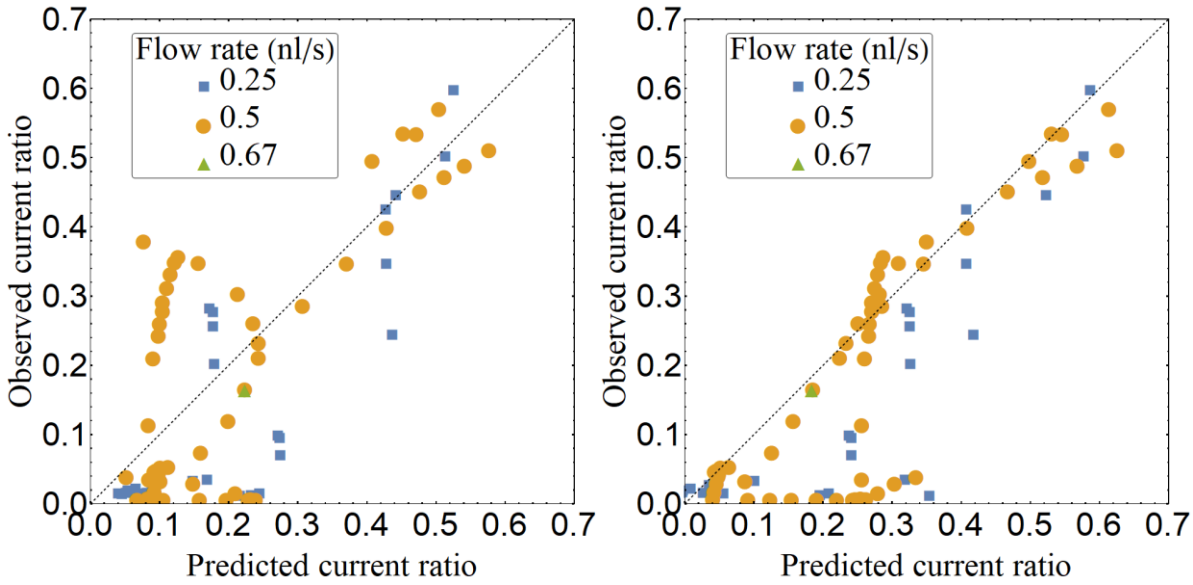

Figure 5: Response curves for the scaling law for extractor current using the linear fit for the calibration coefficient (left) and the inverse power law (right) from Table 3.

VI. Discussion

We have shown in the above investigation that it is possible to develop a simple analytical scaling law for the intercepted extractor current based on a combination of first principles and empirical calibration. As mentioned briefly in the previous section, however, there are caveats to the predictive capabilities of these models. Most notably, we find that there are overall higher deviations between observations and predictions at low extractor-to-beam current ratios (Fig. 5). This result may in part be explained by violations of the key assumptions underlying the derivation outlined in Sec. III. At low current ratios, only the very edges of the beam intercept the extractor. As has been shown by Chiu et al., however, it is in this very region that the assumptions of mono-dispersivity are violated: ions selectively appear in the wings of the plume [20]. Thus, it is not unexpected that the scaling laws fail when only this edge region of the plume intercepts the extractor. With that said, while improved agreement may ultimately be found at these marginal cases by introducing additional terms in the to allow for poly-dispersivity, we note that our result still has utility for evaluating current collection (and, therefore, mass accumulation) in the more egregious, high-risk cases (i.e. higher collected current).

As an additional consideration, we recognize that the results presented in the previous section are not comprehensive. The study was performed for one propellant with one capillary geometry and a fixed extractor diameter. While there are predictions for the effects of propellant properties (as encapsulated in the effective resistance $R_0(P)$ we introduced in Eq. (6)) and extractor width (through the angle ϕ), it remains to be seen if these predictions are valid. Moreover, physically, we may anticipate that the radius of the capillary (and, consequently, the Taylor cone) will also affect divergence, though this does not appear explicitly in our derivation in Sec. III. The role of these parameters could be addressed with an expanded study over multiple geometries and propellant types.

Despite these acknowledged limitations, the results we have presented in the previous section can yield meaningful physical insight. In particular, if we insert the inverse empirical law for the calibration we identified in Table 3 into Eq. (6) for divergence angle, we find the simplified expression:

$$\theta \approx \tan^{-1}\left(\left(R_0(P)\left(\frac{l_0}{d}\right)\frac{I_B}{V_C}\right)^{\frac{3}{4}}\right), \tag{7}$$

where have an introduced a characteristic length, $l_0 \sim a \sim 42$ nm (Table 3). Returning to the interpretation of Lozano [14], the beam divergence is assumed to be driven by the space charge effect in the beam forcing outward radial expansion. The actual angle results from the balance between this space charge field and acceleration by the applied

extractor potential accelerating particles downstream. The previous model [14] assumed that the acceleration occurred entirely in the vicinity of the cone tip, thereby eliminating any dependence of the applied field on extractor gap. Our result re-introduces this dependency, suggesting the axial electric field downstream of the emission site may be finite, an effect that will facilitate the curving of ion trajectories toward the central axis of emission. Practically, this result suggests that moving extractors farther downstream (provided the potential remains sufficiently strong to induce cone emission) will reduce the divergence angle.

As a final comment, we note that the above work has direct implications for the larger goal of identifying simplified scaling laws that can facilitate rapid assessment of critical operational properties such as electrospray life. Indeed, much as there exist scaling laws for current and thrust of these devices, we now have provided a new, empirically-validated expression for intercepted beam current and divergence. As we discussed in Sec. III, provided the beam is approximately mono-dispersive, these expressions can be leveraged to estimate mass accumulation on the extractor (and, therefore, predict failure events). Building on this capability, we also note that although we have confined our analysis to a consideration of the "best-fit" calibrated coefficient, there is an evident spread in the data (as can be seen from Fig. 4). This implies uncertainty in the coefficients for our empirical model. Rigorously, this uncertainty can be incorporated into the scaling law and used to generate assessments of confidence in the predictions for the extractor current collection. This type of uncertainty quantification is the focus of our ongoing efforts to develop robust numerical tools that predict with confidence intervals the lifetime of these systems. Future efforts will focus on incorporating these types of scaling laws with uncertainty into the numerical framework of the ESPET code [16].

VII. Conclusion

In this paper, we have discussed a major life-limiting mechanism for electrospray devices — the impingement of propellant on the downstream extractor electrode — and identified the propellant plume divergence angle as a key factor by which it is shaped. We have argued that, subject to the assumption of a mono-dispersive beam, the extractor current can be used a proxy for this mass accumulation. We in turn have proposed an analytical model based on first principles for this intercepted current under the assumption that the beam expansion is driven by space-charge effects. We similarly have accounted for intuitive but unknown dependence of this divergence on geometry by introducing a calibration coefficient. By employing a parametric experimental investigation, we were able to determine a functional form for this calibration coefficient as it depends on the tip-to-extractor distance. When we combined this expression with our first-principles scaling law for current impingement, we were able to generate model predictions qualitatively and quantitatively consistent with the measured intercepted current on the extractor. These results lend themselves to the physical interpretation that as the distance from tip to extractor is expanded, the applied electric field between the two becomes more longitudinal, facilitating a greater collimation of the beam. Although the scope of this investigation is confined to one type of emitter and propellant, this result does provide scaling parameters that can be verified against other experimental configurations. Similarly, in the larger context of generating simple yet robust scaling laws for electrospray emitter operation, our finding represents a critical step in developing numerical tools to evaluate one of the most dominant life-limiting mechanisms of these devices: mass accumulation on the downstream electrode.

Acknowledgments

The authors are grateful for the helpful discussions from Prof. Alex Gorodetsky, Dr. Rainer Dressler, Mr. Benjamin St. Peter, and Dr. John Yim. The authors also would like to acknowledge the assistance of Mr. Eric Viges in operating and maintaining the experimental facility. This work was supported by an Early Stage Innovations grant from NASA's Space Technology Research Grants Program.

References

[1] Taylor, G. I. (1964). Disintegration of water drops in an electric field. Proceedings of the Royal Society of London. Series A. Mathematical and Physical Sciences, 280(1382), 383-397.

[2] Gaskell, S. J. (1997). Electrospray: principles and practice. Journal of mass spectrometry, 32(7), 677-688.

[3] Lozano, P. C., Wardle, B. L., Moloney, P., & Rawal, S. (2015). Nanoengineered thrusters for the next giant leap in space exploration. *MRS Bulletin*, *40*(10), 842-849.

[4] Jelem, D., Reissner, A., Seifert, B., Buldrini, N., Wilding, L., & Krejci, D. (2018). Direct thrust and plume divergence measurements of the IFM Nano Thruster. *Advances in Space Research*, *62*(12), 3398-3404.

[5] Gassend, B., Velásquez-García, L. F., Akinwande, A. I., & Martínez-Sánchez, M. (2007, July). A fully integrated microfabricated externally wetted electrospray thruster. In 43rd AIAA/ASME/SAE/ASEE Joint Propulsion Conf..

[6] Kimber, A. M., Jorns, B. A., & Sodano, H. (2018). Dielectric Materials with Deposited Electrode Layers for Electrospray Arrays. In *2018 Joint Propulsion Conference* (p. 4653).

[7] Velásquez-García, L. F., Akinwande, A. I., & Martinez-Sanchez, M. (2006). A planar array of micro-fabricated electrospray emitters for thruster applications. *Journal of Microelectromechanical Systems*, *15*(5), 1272-1280.

[8] Ziemer, J., Marrese-Reading, C., Dunn, C., Romero-Wolf, A., Cutler, C., Javidnia, S., ... & Hsu, O. (2017). Colloid Microthruster Flight Performance Results from Space Technology 7 Disturbance Reduction System.

[9] Thuppul, A., Wright, P., & Wirz, R. E. (2018). Lifetime Considerations and Estimation for Electrospray Thrusters. In *2018 Joint Propulsion Conference* (p. 4652).

[10] Little, B., & Jugroot, M. (2017). Investigation of an Electrospray within a Cold Gas Nozzle for a Dual-Mode Thruster. In 53rd AIAA/SAE/ASEE Joint Propulsion Conference (p. 5038).

[11] Wright, P., Thuppul, A., & Wirz, R. E. (2018). Life-Limiting Emission Modes for Electrospray Thrusters. In *2018 Joint Propulsion Conference* (p. 4726).

[12] Ziemer, J. K., Randolph, T. M., Franklin, G. W., Hruby, V., Spence, D., Demmons, N., ... & Connolly, W. (2010, March). Colloid micro-newton thrusters for the space technology 7 mission. In *2010 IEEE Aerospace Conference* (pp. 1-19). IEEE.

[13] Gamero-Castaño, M. (2008). The structure of electrospray beams in vacuum. *Journal of Fluid Mechanics*, *604*, 339-368.

[14] Lozano, P., & Martínez-Sánchez, M. (2003). *Studies on the ion-droplet mixed regime in colloid thrusters* (Doctoral dissertation, PhD dissertation, MIT, Department of Aeronautics and Astronautics, 2003. 29).

[15] Chakraborty, S., Ataman, C., Dandavino, S., & Shea, H. (2012). Microfabrication of an electrospray thruster for small spacecraft. Proceedings of POWERMEMS, 2-5.

[16] St. Peter, B., Dressler, R.A., Chiu, Y.H., Fedkiw, T., Wang, Y. and Song, H. Electrospray Propulsion Engineering Toolkit (ESPET). 2017.

[17] de la Mora, J. F., & Loscertales, I. G. (1994). The current emitted by highly conducting Taylor cones. *Journal of Fluid Mechanics*, *260*,155–184.

[18] Ganan-Calvo, A. M., Davila, J., & Barrero, A. (1997). Current and droplet size in the electrospraying of liquids. Scaling laws. Journal of Aerosol Science, 28(2), 249-275.

[19] ESPET, ElectroSpray Propulsion Engineering Toolkit, Software Package, Spectral Sciences Inc., Burlington, MA.

[20] Chiu, Y., Gaeta, G., Heine, T., Dressler, R., and Levandier, D. "Analysis of the electrospray plume from the EMI-Im propellant externally wetted on a tungsten needle." In *42nd AIAA/ASME/SAE/ASEE Joint Propulsion Conference & Exhibit*, p. 5010, 2006.